Phase-Field Modeling of Solid Electrolyte Interphase (SEI) Evolution: Considering Cracking and Dissolution during Battery Cycling

ECS Transactions, 89 (1) 101-111 (2019)
10.1149/08901.0101ecst ©The Electrochemical Society

Phase-field Modeling of Solid Electrolyte Interphase (SEI) Evolution: Considering Cracking and Dissolution during Battery Cycling

Lin Liu, Pengjian Guan

Department of Mechanical Engineering, University of Kansas, Lawrence, Kansas 66045, USA

The Lithium-ion battery (LIB) degrades over time, which compromises its electrochemical performance and mechanical integrity, eventually battery safety. The evolution of solid electrolyte interphase (SEI) layer is one of the main reasons for the above degradation. The performance and longevity of LIB highly depend on the stability of the SEI. Unfortunately, the SEI layer is not electrochemically and mechanically stable due to the dissolution and cracking of the SEI during battery cycling. In this paper, a phase field model is developed to provide insight into the interaction of cracking and dissolution of the SEI layer. SEI layer experiences stress concentration and de/intercalation, which lead to the cracking of layer; meanwhile, the SEI species may have further reactions with the electrolyte which may lead to dissolution. The cracking of the SEI layer can result in more surfaces to react with electrolyte and further dissolution.

Introduction

Lithium-ion batteries (LIBs) are becoming ubiquitous in portable electronics and transportation energy storage systems (1). Market research suggests that the $23.51 billion-a-year (2015) world-wide LIB market could reach $68.97 billion-a-year by 2022 (2). Meanwhile, many evolving rechargeable batteries (e.g., Mg,(3) and Li Metal(4)), which may be considered as "beyond Lithium-ion batteries," have been intensively researched due to their inherent reversibility and convenient modification of their physicochemical properties (5). Although promising, both LIBs and beyond LIBs suffer from severe degradation and failure mainly at, or near to, the electrode/electrolyte interface. It is believed that those degradation reactions cause severe performance degradation which can be classified into chemical degradation and mechanical degradation (6-10), such as undesired chemical reactions (11), corrosion (12-14), passivation layer formation and growth (15-31), and electrolyte decomposition (32). Among them, the undesired chemical reactions and electrolyte decomposition can result in the formation of a passivation layer called solid electrolyte interphase (SEI) forming and growing at electrode/electrolyte interface (18, 20). While SEI layer growth can cause battery capacity fade and increase cell internal resistance, the SEI can also prevent the exfoliation of electrode materials and inhibit further electrolyte decomposition (33-36). The performance and longevity of LIB highly depend on the stability of the SEI. Unfortunately, it is believed that the SEI layer is not electrochemically and mechanically stable due to the dissolution and cracking of itself during cycling (15, 18, 22, 23, 37). Therefore, a better understanding of the mechanical

degradation and transport properties of the SEI, especially when considering its dissolution and cracking, is necessary, which is the topic of this study.

Once the dissolution occurred, the SEI layer evolves as well. Based on nucleation theory, if the radius of the SEI species is smaller than the critical radius which occurs in the equilibrium state, the SEI species may tend to shrink and eventually dissolve into the electrolyte solution (18, 38). It is believed that the SEI layer has a compact-porous-layered structure. The inorganic compounds are mostly in the compact layer, and the organic compounds are mostly in the porous layer (18). The inorganic compounds are unlikely to dissolve during battery cycling while the dissolution tends to occur within organic compounds (39-42). In addition to the dissolution, SEI layer fracture may also happen due to either of its unstable structure or the cracking of the SEI species (43). The concentration gradient during the transport of lithium-ion can lead to the diffusion-induced stress which can cause stress concentration as well as cracking (44-50). Miehe *et al.* developed a diffusive crack model with a geometric approach to simulate the cracking of electrodes (51). Recently, a core-shell model was built by Deshpande *et al*. to calculate stresses in the SEI layer as well as its fracture (52). The above studies, among many others, are based on Linear Elastic Fracture Mechanics (LEFM), in which the stress at the crack tip is regarded to be sharp with infinite large stress or singular. The stress singularity arises from the linear elastic continuum simplification of materials while assuming a sharp crack tip. The above assumptions may not be applicable to batteries as only a finite value of stress can be resisted by the battery material. The crack tip in batteries may experience intense deformation and develop a finite separation near its tip, which also leads to the redistribution of the high stress. In this work, instead of adopting a sharp crack tip, diffusive interphase is assumed to be governed by a dimensionless phase-field variable. A phase field model is developed to provide insight into the interaction of cracking and dissolution of the SEI layer. In order to reduce the complexity of numerical simulation, volumetric expansion is not considered. The $LiMn_2O_4$ cathode is selected since its volumetric expansion is much smaller compared to the anode (e.g., graphite and silicon) and it has been well studied, which can provide detailed material properties. Figure 1 schematically shows a typical particle agglomeration that is used in the simulation.

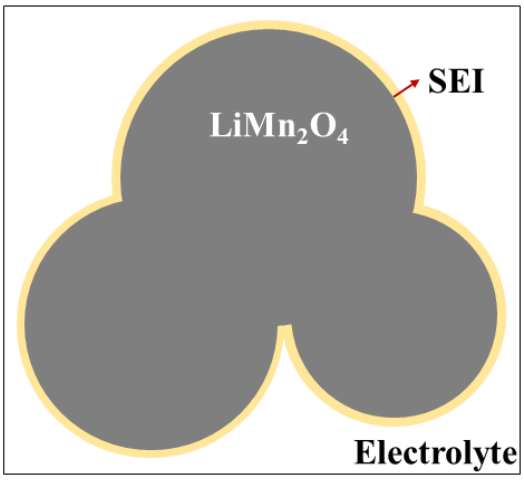

Figure 1: Schematic diagram of particle agglomeration

Methodology

In order to investigate the dissolution and cracking of the SEI layer, the microstructure of SEI should be simulated to obtain firstly. In detail, a phase field variable (φ) represents the solid/liquid volume fraction (V_f) at the electrode/SEI/electrolyte interface.

$$\varphi\ (C_i,t)=2V_f-1 \quad [1]$$

The V_f varies from 0 to 1, where $V_f = 0$, 1 represents the liquid and solid phase, respectively. Similarly, $\varphi\ (C_i,t) = -1$ represents a liquid electrolyte phase, $\varphi\ (C_i,t) = 1$ represents a solid SEI specie, and $-1 < \varphi < 1$ represents the SEI/electrolyte interphase. The Ginzburg-Landau form is applied for the total free energy density:

$$f_{tot} = \frac{1}{2}\lambda|\nabla\varphi|^2 + f_0(\varphi)^2 \quad [2]$$

where f_{tot} is the total free energy density, λ is the free energy gradient, and f_0 is a function of the bulk energy density,

$$f_0 = \frac{\lambda}{4\varepsilon^2}\left(\varphi^2-1\right)^2 \quad [3]$$

The above double-well function is commonly adopted when the phase field model is applied for interphase tracking purposes and represents an approximation of the Van der Waals Equation of State near the critical radius, R_i*(38). In a solid/liquid two-phase system, the total free energy density can be divided into surface free energy density and volume free energy density. The total free energy reaches its maximum value when an SEI species *i* has a critical radius R_i*. If the radius of SEI species R_i is larger than R_i*, volume free energy density is dominant, and the SEI species *i* may tend to grow since the total free energy density is increasing. On the other hand, if R_i is smaller than R_i*, the surface free energy density is dominant, and the SEI species *i* may tend to shrink and eventually dissolve into the electrolyte solution since the total free energy density is decreasing. Yue et al. theoretically investigated the calculation of the critical radius. Their results indicated that changes in the size of solid species are proportional to the thickness of interphase interface ε (38, 53). As $\varepsilon \to 0$, the ratio λ/ε obtains the surface tension coefficient, σ_{se},

$$\sigma_{se} = \frac{2\sqrt{2}}{3}\frac{\lambda}{\varepsilon} \quad [4]$$

In this work, it is assumed that the SEI layer is formed by different precipitated solid species in the electrolyte. As a result, the SEI/electrolyte interface tends to be spherical so as to minimize the surface free energy density. Figure 2 shows a schematic of the contact angle and surface tension coefficients. Young's equation is applied to connect the contact angle (θ) with the SEI/electrolyte interfacial tension coefficient (σ_{se}), the SEI/electrode surface tension coefficient (σ_{sg}), and the electrolyte/graphite surface tension coefficient (σ_{eg}).

$$\cos(\theta) = \frac{\sigma_{sg} - \sigma_{eg}}{\sigma_{se}} \quad [5]$$

Thus, the surface free energy density can be represented as:

$$f_s = \sqrt[3]{4\pi R_i^2}(2\sigma_{se} + \sigma_{sg}) \quad [6]$$

where R_i is the initial radius of the SEI species i.

The phase field variable (φ) herein is a conserved property since the concentration field is a conserved property during long-range diffusion. Therefore, the evolution of φ can be governed by the Cahn-Hilliard equation:

$$\frac{\partial \varphi}{\partial t} + \mathbf{v} \cdot \nabla \varphi = \gamma \nabla^2 \omega \quad [7]$$

where **v** is the flow velocity for the advection and γ is the mobility of the interface with a range of $0 \leq \gamma \leq 1$. γ is used to determine the time scale of Cahn-Hilliard diffusion and control the minimization of the total free energy density. Here ω is the chemical potential coefficient of SEI species:

$$\omega = \lambda \frac{\delta(f_{tot})}{\delta \varphi} \quad [8]$$

$$\omega = \frac{\lambda}{\varepsilon^2}\left[-\varepsilon^2 \cdot \nabla^2 \varphi + \varphi(\varphi^2 - 1)\right] \quad [9]$$

The Cahn-Hilliard equation forces φ to take either value of 1 or −1, and can be represented by two second-order PDEs:

$$\frac{\partial \varphi}{\partial t} + \mathbf{v} \cdot \nabla \varphi = \frac{\gamma \lambda}{\varepsilon^2} \nabla^2 \phi \quad [10]$$

$$\phi = -\nabla \cdot \varepsilon^2 \nabla \varphi + (\varphi^2 - 1)\varphi \quad [11]$$

Once its microstructure obtained, the SEI layer is considered to be an α phase. The electrolyte is treated as another β phase. Two of the phase field variables are utilized herein. The phase field variable φ_c represents the fracture and changes from 0 to 1. $\varphi_c = 0$ represents a fully broken crack in the SEI, while $\varphi_c = 1$ represents a completely intact of the SEI. φ_c from 0 to 1 represents the transitional regions. The phase field variable X_i is related to the Li-ion concentration. X_1 is the mole fractions of Li-ions in the SEI phase. X_2 is the mole fraction of Li-ions in the electrolyte phase.

Therefore, the total free energy of an isothermal system can be represented as:

$$E = \int_V [f_V(\varphi;X_1,X_2,X_3;T)+(\sum_{i=1}^{2} w_i X_i)\, g(\varphi_c)+\frac{1}{2}k^2|\nabla\varphi_c|^2+\frac{1}{2}\rho\epsilon+f_u]dV \quad [12]$$

where f_V is the bulk free energy per unit volume and T is the absolute temperature. The second term in this equation is the potential well at the interphase between electrolyte and SEI species. The coefficients w_i are determined by the energy barriers for changed species to pass through the interphase. The third term is the gradient energy, where k is the gradient energy coefficient for the phase field. The fourth term denotes the electrostatic energy, where ϵ is the electrostatic potential and the charge density ρ can be represented as:

$$\rho = \frac{F}{\Omega}\sum_{i=1}^{n} z_i X_i \quad [13]$$

where Z_i is the valence of species, and F is the Faraday's constant. The last term f_u is the elastic strain energy density is calculated by:

$$f_u = d(\varphi_c)\left(\xi_s-\xi_c\right)+\xi_c \quad [14]$$

where $d(\varphi_c)$ describes the coupling between the fracture phase field variable and the elastic strain field, this is determined by:

$$d(\varphi_c) = \varphi_c{}^3(4-3\varphi_c) \quad [15]$$

where ξ_s is the elastic strain energy density:

$$\xi_s = \frac{Yv}{2(1+v)(1-2v)}(\varepsilon_{ii})^2 + \frac{Y}{2(1+v)}\varepsilon_{ij}\varepsilon_{ij} - \frac{1}{3}\frac{Y\Omega}{1-2v}c_{\max}c\varepsilon_{ii} \quad [16]$$

where Y and v are Young's modulus and Poisson's ratio, respectively. ξ_c is a threshold value taking the form of $\xi_c = E\varepsilon_c{}^2$, where ε_c is the threshold strain.

The bulk-free energy density can be represented as:

$$f_v(\varphi_c\varphi,X_i,T) = f_{\varphi_c}+f_X \quad [17]$$

$$f_{\varphi_c}=16hg(\varphi_c) \quad [18]$$

$$g(\varphi_c) = \varphi_c{}^2(1-\varphi_c)^2 \quad [19]$$

where f_X is the free energy density of the system with concentration c, which is discussed in our previous paper (18). The choice of bulk free energy density function can have a significant effect on the physical behavior of the interphase. In this work, a double-well function $f_{\varphi c}$ is applied with an energy barrier of height h. The physical justification of $f_{\varphi c}$ comes from the separation of phases into domains of pure components.

The charge transport and microstructure evolution can also be represented with the equations listed below by minimizing the total free energy of the system. Depending on whether the phase field variable is assumed to be conserved or non-conserved, the dynamic evolution of the phase field variable can be derived to be of the form of Cahn-Hilliard equation or the Ginzburg-Landau equation. Since the characteristic time of the elastic field is much less than the other concentration field and fracture field, the evolution equation of the displacement can be regarded as quasi-static. Therefore, the Ginzburg-Landau equation is solved to derive the governing equations of the system which controls the evolution of non-conserved phase field variable φ_c. The Cahn-Hilliard equation is solved to derive the governing equations of the system which controls the evolution of conserved phase field variable X_i:

$$\frac{\partial X_i}{\partial t} = \nabla \cdot \left[M_i(r) \cdot \nabla \frac{\delta E}{\delta X_i} \right] \quad [20]$$

$$\frac{\partial \varphi_c}{\partial t} = -L \frac{\delta E}{\delta \varphi_c} \quad [21]$$

$$M_i(r) = \frac{(1 - X_i) X_i D_i}{RT} \quad [22]$$

where $M_i(r)$ is the mobility tensor of the ith species, L is the interface mobility of phase field variable φ and D_i is the diffusivity of the species.

In addition, the flux vector, J is assumed to be proportional to the gradient of the chemical potential $\nabla\mu$.

$$J = -Mc\nabla\mu \quad [23]$$

The chemical potential can be represented as:

$$\mu = \mu_0 + N_A c_{\max} k_B T \ln c \quad [24]$$

where μ_0 is a constant, N_A is the Avogadro's constant, and k_B is the Boltzmann constant. Then, the flux vector J can be rewritten as:

$$J = -MN_A c_{\max} k_B T \nabla c + Mck_c \nabla \nabla^2 c + Mc\Omega c_{\max} \nabla \sigma \quad [25]$$

where σ is the hydrostatic stress.

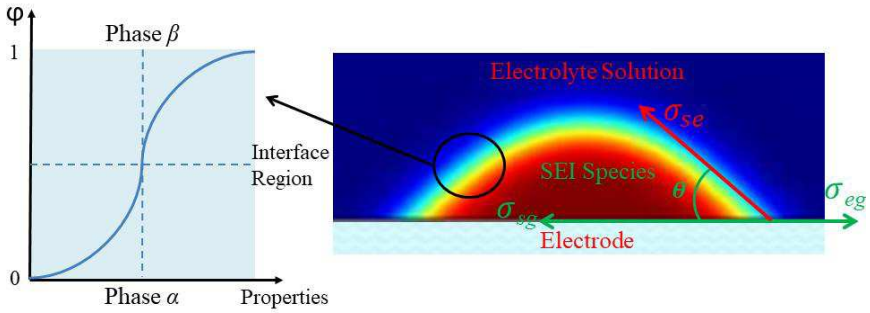

Figure 2: Schematics of phase field variable and contact angle with the surface tension coefficients of SEI species

Results and Discussion

During battery cycling, the elastic strain energy density is affected by the lithium ion diffusion and concentration, as described in Eqn [16]. Figure 3 presents the distribution of lithium ion concentration in the $LiMn_2O_4$ particle agglomeration at different potentials. When the battery is fully discharged at 2.51V, the concentration will reach the highest level inside the particle agglomeration. Material properties and cycling conditions can be found in our previous work (54-56). The concentration gradient can cause diffusion-induced stress. Also, the lithium-ion diffuses from the region with lower hydrostatic stress to somewhere have higher hydrostatic stress. Hence, the locations with higher lithium ion concentration are chosen for SEI microstructure simulation.

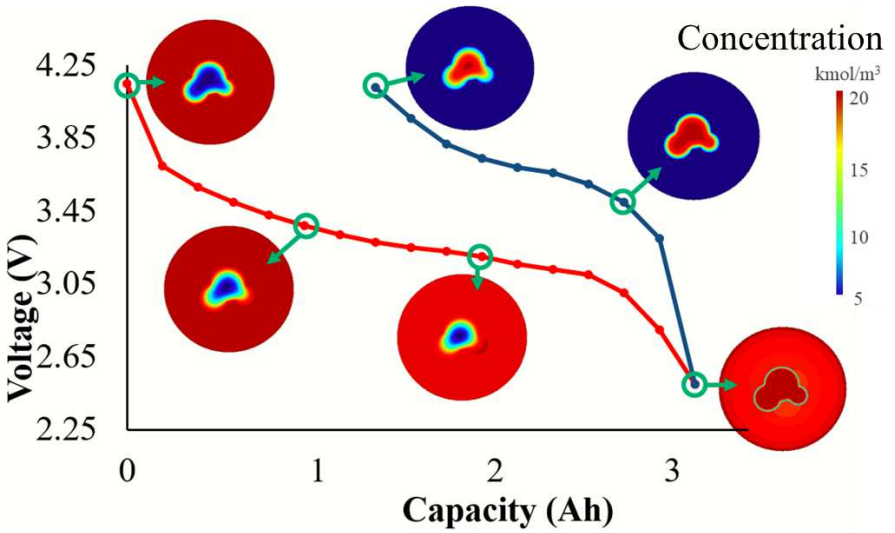

Figure 3: Lithium-ion concentration distribution during cycling

Once the lithium-ion concentration profile obtained, the SEI microstructure can be simulated to obtain. The formation and morphology evolution of SEI are simplified as a solidification process. Figure 4 shows the SEI microstructure and its morphology evolution. Initially, the electrolyte solution becomes unstable, and reduction reactions happen with electrons from the electrode to form SEI species (solid phase) in the electrolyte solution (liquid phase) that may undergo decomposition. SEI species accumulate and form a passivation layer with a compact-porous-layered structure that hinders direct contact

between the electrolyte solution and electrode surface. Since the porous SEI layer has lower electronic conductivity than the compact layer, it will stop growing when the electrolyte solution molecules can no longer receive electrons from the electrode to be further reduced. Consequently, SEI growth rate reduces and SEI layer stabilizes.

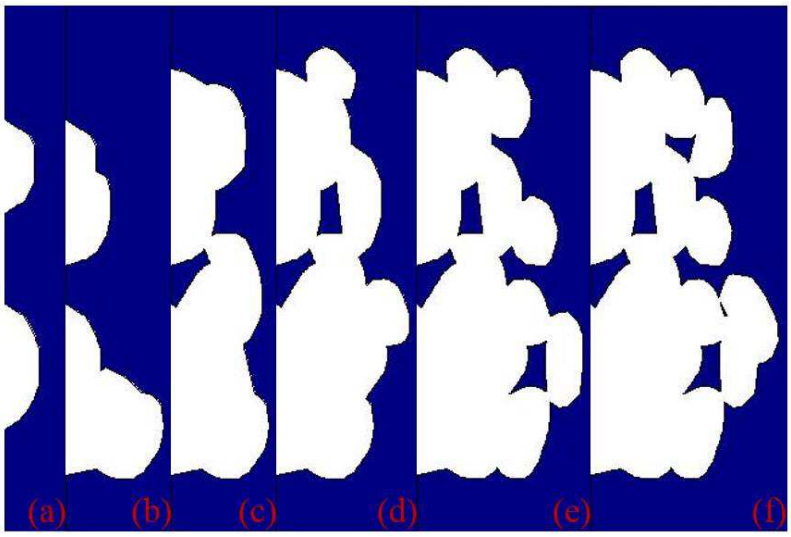

Figure 4: SEI species and layer formation and growth at different times (a: t = 1.8 μs, b: t = 7.2 μs, c: t = 12.6 μs, d: t = 16.2 μs, e: t = 19.8 μs, f: t = 28.8 μs)

In order to investigate how cracks affect each other when they are close, two special cases are studied, i.e., vertical cracks and horizontal cracks, as shown in Figure 5. The highest stress of the vertical crack is greater than the highest stress of the horizontal crack. Therefore, the vertical crack grows up faster than the horizontal crack at the beginning. The vertical crack and the horizontal crack trend to coalesce into a single large crack. The center part of the horizontal crack coalesces into the vertical crack, growing much larger than both ends. Meanwhile, the crack propagation of two parallel cracks is also simulated. The two cracks trend to coalesce toward the center of the crack.

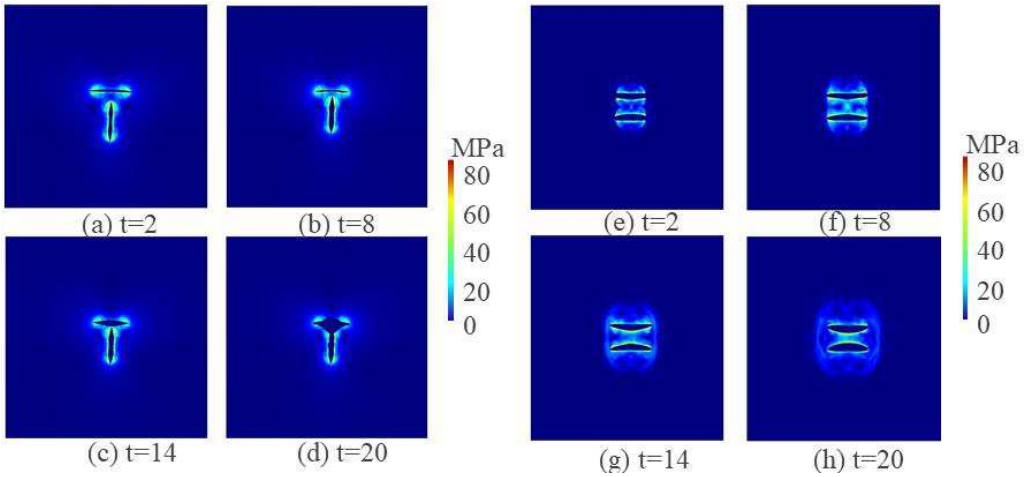

Figure 5: Crack propagation with two vertical cracks and two parallel cracks (Unit of time: 10^2 seconds)

After training the model with above crack propagation analysis, the cracking of the SEI can be applied to the SEI microstructure obtained, as shown in Figure 6. The porous layer

which is mostly formed by inorganic compounds and tends to dissolve faster than the compact layer during the charging and discharging cycles. In Figure 6(c), the cracks start to penetrate the boundaries of the SEI species. In Figure 6(d), the cracks tend to grow into each other if they keep growing and become close enough.

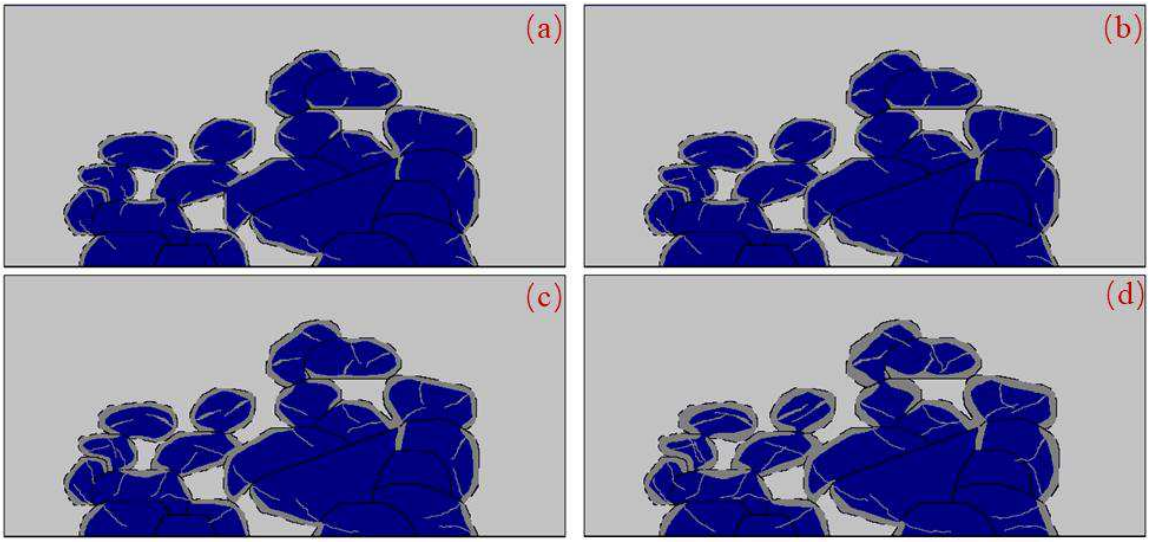

Figure 6: Dissolution and Cracking of the SEI at (a) 50 cycles, (b) 100 cycles, (c) 150 cycles, and (d) 200 cycles.

Conclusion

In this work, a phase field model has been developed to investigate cracking and dissolution of the SEI during battery cycling. In a non-homogenous system, the hydrostatic gradient stress can lead to the accumulation of lithium ions. Therefore, the SEI will crack first at locations with high lithium-ion concentration levels. In this model, the shape of the SEI species is determined by minimizing the total free energy density of the two-phase system to reach a state of equilibrium. With obtained the lithium ion concentration profile during battery cycling, the SEI microstructure can be obtained via the proposed phase-field modeling. Compared with other models, the phase-field model does not need to track the interfaces directly. In addition, multiple phase-field variables have been applied to predict lithium-ion diffusion, cracking and dissolution of the SEI layer. With considering the variation of lithium ion concentration during battery cycling, the developed phase-field model will strengthen the current understanding of SEI microstructure evolution. Currently, we focus on experimental validation of the proposed model, and further investigate the interaction effect of cracking and dissolution on battery performance experimentally.

Acknowledgments

This work was supported by the National Science Foundation under Grant Number 1840732. In the meanwhile, the authors would like to thank the support from KS NASA EPSCoR program and KU General Research Fund.

References

1. M. Armand and J. M. Tarascon, *Nature*, **451**, 652 (2008).
2. Lithium Ion Battery Market by Type, Power Capacity, Industry, and Geography - Global Forecast to 2022, in, MarketsAndMarkets (2017).
3. P. Saha, M. K. Datta, O. I. Velikokhatnyi, A. Manivannan, D. Alman and P. N. Kumta, *Progress in Materials Science*, **66**, 1 (2014).
4. Y. Liu, Q. Liu, L. Xin, Y. Liu, F. Yang, E. A. Stach and J. Xie, **2**, 17083 (2017).
5. M. S. Whittingham and L. B. Ebert, in *Intercalated Layered Materials*, p. 533, Springer (1979).
6. M. K. S. Verma, S. Basu, K. S. Hariharan, S. M. Kolake, T. Song and J. Jeon, *Journal of The Electrochemical Society*, **164**, A3426 (2017).
7. C. Liu and L. Liu, *ECS Transactions*, **77**, 257 (2017).
8. C. Liu and L. Liu, *Journal of The Electrochemical Society*, **164**, E3254 (2017).
9. C. Liu and L. Liu, *Meeting Abstracts*, **MA2017-01**, 326 (2017).
10. M. Moradi and L. Liu, *Meeting Abstracts*, **MA2015-02**, 216 (2015).
11. P. Arora, R. E. White and M. Doyle, *Journal of the Electrochemical Society*, **145**, 3647 (1998).
12. E. Cho, J. Mun, O. B. Chae, O. M. Kwon, H.-T. Kim, J. H. Ryu, Y. G. Kim and S. M. Oh, *Electrochemistry Communications*, **22**, 1 (2012).
13. A. Abouimrane, J. Ding and I. J. Davidson, *Journal of Power Sources*, **189**, 693 (2009).
14. S. S. Zhang and T. R. Jow, *Journal of Power Sources*, **109**, 458 (2002).
15. F. M. Wang, M. H. Yu, Y. J. Hsiao, Y. Tsai, B. J. Hwang, Y. Y. Wang and C. C. Wan, *International Journal of Electrochemical Science*, **6**, 1014 (2011).
16. H. Schranzhofer, J. Bugajski, H. J. Santner, C. Korepp, K. C. Möller, J. O. Besenhard, M. Winter and W. Sitte, *Journal of Power Sources*, **153**, 391 (2006).
17. J. Yan, B.-J. Xia, Y.-C. Su, X.-Z. Zhou, J. Zhang and X.-G. Zhang, *Electrochimica Acta*, **53**, 7069 (2008).
18. P. Guan, L. Liu and X. Lin, *Journal of The Electrochemical Society*, **162**, A1798 (2015).
19. P. Guan and L. Liu, *Meeting Abstracts*, **MA2015-02**, 268 (2015).
20. P. Guan and L. Liu, *ECS Transactions*, **66**, 81 (2015).
21. P. Guan and L. Liu, *MRS Proceedings*, **1753** (2015).
22. L. Liu, P. Guan and C. Liu, *Journal of The Electrochemical Society*, **164**, A3163 (2017).
23. L. Liu and P. Guan, *ECS Transactions*, **77**, 321 (2017).
24. P. Guan and L. Liu, *Meeting Abstracts*, **MA2017-01**, 355 (2017).
25. C. Liu and L. Liu, *ECS Transactions*, **69**, 5 (2015).
26. C. Liu and L. Liu, *International Journal of Hydrogen Energy*, **40**, 8454 (2015).
27. C. Liu and L. Liu, *Meeting Abstracts*, **MA2015-02**, 353 (2015).
28. L. Liu, J. Park, X. Lin, A. M. Sastry and W. Lu, *Journal of Power Sources*, **268**, 482 (2014).
29. L. Liu and M. Zhu, *ECS Transactions*, **61**, 43 (2014).
30. X. Lin, L. Liu and P. Guan, *Meeting Abstracts*, **MA2014-01**, 32 (2014).
31. X. Lin, J. Park, L. Liu, Y. Lee, A. M. Sastry and W. Lu, *Journal of The Electrochemical Society*, **160**, A1701 (2013).
32. K. Leung, S. B. Rempe, M. E. Foster, Y. Ma, J. M. M. del la Hoz, N. Sai and P. B. Balbuena, *Journal of the Electrochemical Society*, **161**, A213 (2014).

33. H. Jannesari, M. D. Emami and C. Ziegler, *Journal of Power Sources*, **196**, 9654 (2011).
34. A. M. Colclasure, K. A. Smith and R. J. Kee, *Electrochimica Acta*, **58**, 33 (2011).
35. R. Srinivasan and B. G. Carkhuff, *Journal of Power Sources*, **241**, 560 (2013).
36. G. K. Prasad and C. D. Rahn, *Journal of Power Sources*, **232**, 79 (2013).
37. M. Ulldemolins, F. Le Cras, B. Pecquenard, V. P. Phan, L. Martin and H. Martinez, *Journal of Power Sources*, **206**, 245 (2012).
38. P. Yue, C. Zhou and J. J. Feng, *Journal of Computational Physics*, **223**, 1 (2007).
39. S. J. An, J. Li, C. Daniel, D. Mohanty, S. Nagpure and D. L. Wood, *Carbon*, **105**, 52 (2016).
40. A. Kinaci, H. Yildirim, J. Greeley and M. K. Y. Chan, *Meeting Abstracts*, **MA2015-01**, 288 (2015).
41. F. A. Soto, A. Marzouk, F. El-Mellouhi and P. B. Balbuena, *Chemistry of Materials*, **30**, 3315 (2018).
42. H. Shin, J. Park, S. Han, A. Sastry and W. Lu, *Component-/structure-dependent elasticity of solid electrolyte interphase layer in Li-ion batteries: Experimental and computational studies* (2015).
43. A. Verma and P. P. Mukherjee, *Journal of The Electrochemical Society*, **164**, A3570 (2017).
44. N. Kotak, P. Barai, A. Verma, A. Mistry and P. P. Mukherjee, *Journal of The Electrochemical Society*, **165**, A1064 (2018).
45. P. Zuo and Y.-P. Zhao, *Physical Chemistry Chemical Physics*, **17**, 287 (2015).
46. X. Zhang, W. Shyy and A. Marie Sastry, *Journal of The Electrochemical Society*, **154**, A910 (2007).
47. J. Cho, *Journal of Materials Chemistry*, **20**, 4009 (2010).
48. L. Liu and C. Liu, *Meeting Abstracts*, **MA2018-01**, 1964 (2018).
49. L. Liu and M. Moradi, *ECS Transactions*, **77**, 273 (2017).
50. M. Moradi and L. Liu, *Meeting Abstracts*, **MA2017-01**, 327 (2017).
51. C. Miehe, H. Dal, L. M. Schänzel and A. Raina, *International Journal for Numerical Methods in Engineering*, **106**, 683 (2016).
52. R. D. Deshpande and D. M. Bernardi, *Journal of The Electrochemical Society*, **164**, A461 (2017).
53. C. Z. P. Yue, J.J. Feng,, *Journal of Computational Physics*, **219**, 47 (2006).
54. P. Guan and L. Liu, *MRS Proceedings*, **1753**, mrsf14 (2015).
55. X. Lin, J. Park, L. Liu, Y. Lee, A. Sastry and W. Lu, *Journal of the Electrochemical Society*, **160**, A1701 (2013).
56. L. Liu, J. Park, X. Lin, A. M. Sastry and W. Lu, *Journal of Power Sources*, **268**, 482 (2014).